12th International Symposium on Turbulence and Shear Flow Phenomena (TSFP12)
Osaka, Japan (Online), July 19-22, 2022

ON IMPLICIT LARGE EDDY SIMULATION IN COMPRESSIBLE TURBULENCE

Guiyu Cao
Southern University of Science and Technology
caogy@sustech.edu.cn

Wenjin Zhao
Hong Kong University of Science and Technology
wzhaoag@connect.ust.hk

Shiyi Chen
Southern University of Science and Technology
chensy@sustech.edu.cn

ABSTRACT

Current research conducts the quantitative comparisons between implicit large eddy simulation (iLES) and static explicit large eddy simulation (eLES). We start with the implementations of iLES and eLES in compressible Taylor-Green vortex problem. Compared with the key statistical quantities of direct numerical simulation (DNS), iLES outweighs eLES on the exactly same unresolved grids. With DNS solution, *priori* analysis of compressible filtered subgrid-scale (SGS) turbulent kinetic energy $\overline{\rho}K_{sgs}^{f}$ provides the following observations: forward and backward filtered SGS turbulent kinetic energy transfer; ensemble turbulent kinetic energy E_k is in the order of $\mathscr{O}(10^4)$ to $\mathscr{O}(10^2)$ of ensemble filtered SGS turbulent kinetic energy K_{sgs}^{f}; ensemble dominant physical dissipation rate ε_1 is approximately 20 times larger than ensemble filtered SGS dissipation rate $-\tau_{ij}^{f}\widetilde{S}_{ij}^{f}$. Then, for iLES and eLES, the total dissipation rate is decomposed into resolved physical dissipation rate ε_{phy}, modeling SGS dissipation rate ε_{sgs}^{mod}, and numerical SGS dissipation rate ε_{sgs}^{num}. Quantitative comparisons on the modeling SGS dissipation rate and numerical SGS dissipation rate in iLES and eLES are implemented. We confirms that the numerical dissipation in iLES can be treated as the built-in SGS dissipation, which accounts for the reasonable performance of iLES. While the explicit modeling SGS dissipation in eLES pollutes the resolved turbulent structures in such low-Reynolds number turbulence. We believe that the next generation of large eddy simulation on unresolved grids must take both the built-in numerical SGS dissipation and its competition explicit modeling SGS dissipation into account.

INTRODUCTION

Large eddy simulation (LES) is proposed to solve the filtered Navier-Stokes equations (NSE) with resolvable turbulent structures above the inertial scale (Manabe *et al.*, 1965). Static explicit large eddy simulation (eLES) has been widely used in unsteady separated turbulent flows (Nicoud & Ducros, 1999; Vreman, 2004; Sagaut, 2006; Garnier *et al.*, 2009). Different with the eLES, implicit large eddy simulation (iLES) takes the built-in numerical dissipation as the subgrid-scale (SGS) dissipation (Boris *et al.*, 1992; Grinstein *et al.*, 2007). Due to the lower computational costs and reasonable performance, iLES has been gradually utilized in LES community (Lombard *et al.*, 2016; Moser *et al.*, 2021).

In the past decades, the finite-volume gas-kinetic scheme (GKS) based on the Bhatnagar-Gross-Krook (BGK) model (Bhatnagar *et al.*, 1954) have been developed systematically for computations from low speed flows to supersonic ones (Xu, 2001, 2015). The GKS presents a gas evolution process from kinetic scale to hydrodynamic scale, where both inviscid and viscous fluxes are recovered from a time-dependent and multi-dimensional gas distribution function at a cell interface. Based on the time-dependent flux, a reliable two-stage framework (Li & Du, 2016) was provided for developing the high-order GKS (HGKS) (Pan *et al.*, 2016). In terms of low-Reynolds number turbulent flows, the HGKS has been used as a direct numerical simulation (DNS) tool (Kumar *et al.*, 2013; Cao *et al.*, 2021*a*, 2022). The numerical performance (i.e., numerical accuracy, robustness) and computational cost is comparable with the widely-used high-order finite difference method (DeBonis, 2013). HGKS also shows advantage in supersonic turbulence studies due to its reliable robustness. HGKS indeed provides a valid tool for the numerical simulation of turbulence, which is much less reported in finite volume scheme.

HGKS has been implemented for the iLES in compressible turbulent flows (Cao *et al.*, 2021*b*), i.e., compressible turbulent flow over periodic hills with volumetric Mach number $Ma_v = 0.2$ and cross-sectional Reynolds number $Re_b = 2800$. Compared with the key statistical quantities of DNS, we found that iLES outweighs eLES on the exactly same unresolved grids. eLES over-predicts the normalized Reynolds stresses and provides much stronger turbulent fluctuation than that of DNS solution. While, the solutions from iLES agree well with the DNS results, and the over-predicted performance seldom appears. Thus, we speculated that the static explicit LES model may pollute the resolved turbulent structures of low-Reynolds number separated turbulent flows. To shed light on the seemingly abnormal performance, current research conducts the quantitative comparisons between iLES and eLES, especially focusing on the numerical SGS dissipation and modeling SGS dissipation.

This paper is organized as follows. After the introduction, HGKS is introduced briefly. Followed by the numerical results and quantitative analysis, the last section presents the conclusion and discussion.

NUMERICAL SCHEME

The three-dimensional BGK equation (Bhatnagar *et al.*, 1954) reads

$$f_t + uf_x + vf_y + wf_z = \frac{g-f}{\tau}, \tag{1}$$

where $\boldsymbol{u} = (u,v,w)^T$ is the particle velocity, f is the gas distribution function, g is the three-dimensional Maxwellian distribution and τ is the particle collision time. Chapman-Enskog expansion (Chapman & Cowling, 1990) provides $\tau = \mu/p$, where μ is the molecular viscosity and p is the pressure. The collision term satisfies the compatibility condition

$$\int \frac{g-f}{\tau}\boldsymbol{\psi}\mathrm{d}\Xi = 0, \tag{2}$$

with $\boldsymbol{\psi} = (1,u,v,w,(u^2+v^2+w^2+\xi^2)/2)^T$, $\xi^2 = \xi_1^2 + ... + \xi_N^2$, $\mathrm{d}\Xi = \mathrm{d}u\mathrm{d}v\mathrm{d}w\mathrm{d}\xi_1 \ldots \mathrm{d}\xi_N$. $N = (5-3\gamma)/(\gamma-1)$ is the internal degree of freedom, and γ is the specific heat ratio.

Taking moments of Eq.(1) and integrating with respect to space, the finite volume scheme can be expressed as

$$\frac{\mathrm{d}(\boldsymbol{Q}_{ijk})}{\mathrm{d}t} = \mathscr{L}(\boldsymbol{Q}_{ijk}), \tag{3}$$

where $\boldsymbol{Q}_{ijk}$ is the vector of conservative variables, namely, density ρ, momentum ρU_i, and total energy ρE. The operator $\mathscr{L}$ is defined as

$$\mathscr{L}(\boldsymbol{Q}_{ijk}) = -\frac{1}{|\Omega_{ijk}|}\sum_{p=1}^{6}\mathbb{F}_p(t), \tag{4}$$

where control volume $\Omega_{ijk} = \bar{x}_i \times \bar{y}_j \times \bar{z}_k$ with $\bar{x}_i = [x_i - \Delta x/2, x_i + \Delta x/2], \bar{y}_j = [y_j - \Delta y/2, y_j + \Delta y/2], \bar{z}_k = [z_k - \Delta z/2, z_k + \Delta z/2]$, $\mathbb{F}_p(t)$ is the numerical flux across the cell interface Σ_p.

The numerical flux in x-direction is given as an example

$$\mathbb{F}_p(t) = \sum_{m,n=1}^{2}\omega_{mn}\int \boldsymbol{\psi}uf(\boldsymbol{x}_{i+1/2,j_m,k_n}, t, \boldsymbol{u}, \xi)\mathrm{d}\Xi\Delta y\Delta z. \tag{5}$$

The Gaussian quadrature is used over the cell interface, where ω_{mn} is the quadrature weight, $\boldsymbol{x}_{i+1/2,m,n} = (x_{i+1/2}, y_{j_m}, z_{k_n})$ and (y_{j_m}, z_{k_n}) is the Gauss quadrature point of cell interface $\bar{y}_j \times \bar{z}_k$. The gas distribution function $f(\boldsymbol{x}_{i+1/2,j_m,k_n}, t, \boldsymbol{u}, \xi)$ in the local coordinate can be given by the integral solution of Eq.(1) as

$$\begin{aligned} f(\boldsymbol{x}_{i+1/2,j_m,k_n}, t, \boldsymbol{u}, \xi) =& \frac{1}{\tau}\int_0^t g(\boldsymbol{x}', t', \boldsymbol{u}, \varsigma)e^{-(t-t')/\tau}\mathrm{d}t' \\ &+ e^{-t/\tau}f_0(-\boldsymbol{u}t, \xi), \end{aligned} \tag{6}$$

where $\boldsymbol{x}' = \boldsymbol{x}_{i+1/2,j_m,k_n} - \boldsymbol{u}(t-t')$ is the trajectory of particles, f_0 is the initial gas distribution function, and g is the corresponding equilibrium state. In GKS framework, the second-order gas distribution function at cell interface has been constructed (Xu, 2001). After the gas distribution function being determined, the numerical flux can be obtained by taking moments of it as Eq.(5). To achieve high-order accuracy in space and time, the high-order spatial reconstruction and the multi-stage time discretization has been systematically developed in Li & Du (2016); Pan *et al.* (2016). In current study, the well-developed in-house three-dimensional (3D) parallel code will be used to provide the high-accuracy flow-fields for iLES and eLES. More details in HGKS can be found in Cao *et al.* (2022).

When implementing the eLES models, an extended BGK equation has been proposed as

$$f_t + uf_x + vf_y + wf_z = \frac{g-f}{\tau+\tau_t}, \tag{7}$$

where τ_t is an enlarged turbulent relaxation time. Based on the Chapman-Enskog expansion, Eq.(7) can recover the eddy viscosity model according to the following relation between turbulent eddy viscosity μ_t and turbulent relaxation time τ_t as

$$\tau + \tau_t = \frac{\mu + \mu_t}{p}, \tag{8}$$

where static Smagorinsky model (S-model) and Vreman-type model (V-model) (Vreman, 2004) are used to obtain the turbulent eddy viscosity μ_t in Eq.(8). The detailed implementations and comparisons among different eddy viscosity models within the HGKS framework has been conducted in Zhao *et al.* (2021). In following study, the S-model is equipped with the coefficient $C_s = 0.1$, and V-model adopts corresponding coefficient as $C_v = 2.5C_s^2 = 0.025$.

RESULTS AND ANALYSIS

In this section, iLES and eLES are implemented in compressible Taylor-Green vortex problem (TGV). *Priori* coarse-grained analysis of DNS solution sheds light on expected modeling SGS dissipation, and the quantitative SGS dissipation analysis will be presented subsequently.

Numerical Simulation in TGV

Taylor-Green vortex is a classical problem in fluid dynamics developed to study vortex dynamics, turbulent transition, turbulent decay and energy dissipation process (Brachet *et al.*, 1983; Gallis *et al.*, 2017). The flow is computed within a periodic square box defined as $-\pi L \le x,y,z \le \pi L$. Fluid is a perfect gas with $\gamma = 1.4$ and Prandtl number $Pr = 1$. Mach number takes $Ma = 0.1$ and Reynolds number is $Re = 1600$. iLES and eLES are simulated in 256^3 grids. The detailed setup can be found in Cao *et al.* (2022).

To evaluate the performance of iLES and eLES, several diagnostic dynamic quantities are computed. The ensemble (volume-averaged) turbulent kinetic energy E_k is

$$E_k = \frac{1}{\rho_0\Omega}\int_\Omega \frac{1}{2}\rho U_i \cdot U_i \mathrm{d}\Omega, \tag{9}$$

where ρ_0 is the initial density, Ω the volume of whole computational domain, $(\cdot)$ the inner product. The ensemble enstrophy dissipation rate $\varepsilon(\zeta)$ is related to the enstrophy ζ as

$$\begin{aligned} \varepsilon(\zeta) &= \frac{2\mu}{\rho_0}\zeta, \\ \zeta &= \frac{1}{\rho_0\Omega}\int_\Omega \frac{1}{2}\rho\omega_i \cdot \omega_i \mathrm{d}\Omega, \end{aligned} \tag{10}$$

where vorticity is $\omega_i = \varepsilon_{ijk}U_{k,j}$ with ε_{ijk} the alternating tensor and $U_{k,j} = \partial U_i/\partial x_j$. $\varepsilon(\zeta)$ is utilized to evaluate the resolution of resolved turbulent structures. For the compressible flow, the ensemble physical dissipation rate ε_{phy} obtained from the NSE is the sum of three contributions

$$\begin{aligned} \varepsilon_{phy} &= \varepsilon_1 + \varepsilon_2 + \varepsilon_3, \\ \varepsilon_1 &= \frac{2\mu}{\rho_0\Omega}\int_\Omega S_{ij}^* : S_{ij}^* \mathrm{d}\Omega, \\ \varepsilon_2 &= \frac{\mu_b}{\rho_0\Omega}\int_\Omega \theta^2 \mathrm{d}\Omega, \\ \varepsilon_3 &= -\frac{1}{\rho_0\Omega}\int_\Omega p\theta \mathrm{d}\Omega, \end{aligned} \tag{11}$$

where S_{ij}^* is the deviatoric part of the strain rate tensor S_{ij}, with $S_{ij}^* = S_{ij}^* - \delta_{ij}S_{kk}/3$, $S_{ij} = (U_{i,j} + U_{j,i})/2$. $(:)$ denotes the product for second-order tensor. μ_b is the bulk viscosity, and the inherent bulk viscosity is $\mu_b = 4\mu/15$ for BGK model (Xu, 2015). $\theta = U_{i,i}$ denotes the divergence of turbulent velocity. To eliminate the post-processing error from numerical discretization, all spatial derivatives in Eq.(10) and Eq.(11) are

computed by sixth-order central difference.

Figure 1 presents the time history of ensemble turbulent kinetic energy E_k. Compared with the DNS solution (Cao *et al.*, 2022), we observe that the first-order statistical variable E_k is not sensitive to the grid resolution, as well as iLES or eLES models. Figure 2 clearly presents that iLES performs better than eLES, entailing iLES resolve much accurate turbulent structures. In current compressible simulation with small Mach number $Ma = 0.1$, Figure 3 shows that primary dissipation rate ε_1 is the dominant contribution to ensemble physical dissipation rate ε_{phy}. Meanwhile, dominant ensemble dissipation rate ε_1 in Figure 3 again to show that iLES outweighs eLES on the exactly same unresolved grids. The similar conclusion has been drawn in previous simulation of compressible separated turbulent flow (Cao *et al.*, 2021*b*), where iLES outweighs eLES in compressible turbulent flow over periodic hills. In terms of ignorable ensemble dissipate rate ε_2 and ε_3, iLES and eLES are in the quite similar performance.

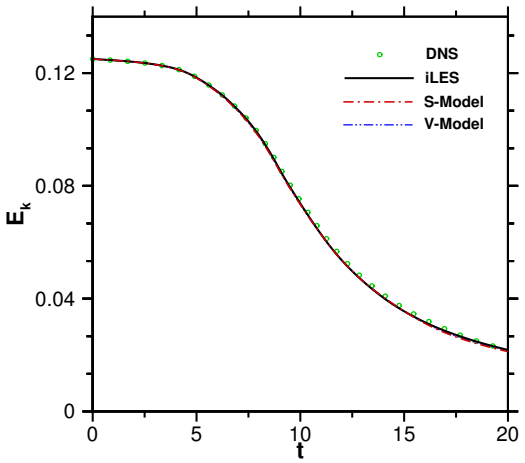

Figure 1. Time history of ensemble turbulent kinetic energy E_k. The DNS solution with 1024^3 grids is provided in Cao *et al.* (2022).

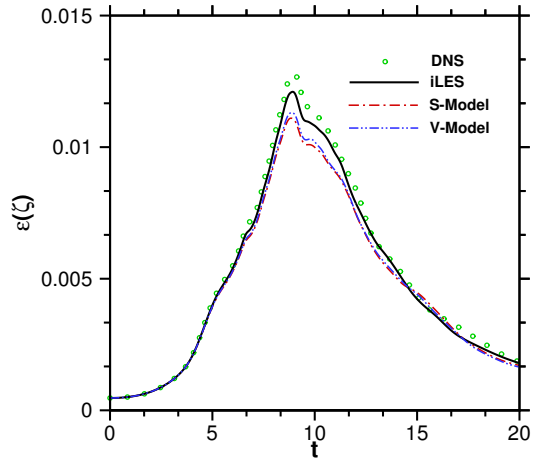

Figure 2. Time history of ensemble enstrophy dissipation rate $\varepsilon(\zeta)$.

Priori Analysis of K^f_{sgs}

To study the seemingly abnormal performance of iLES and eLES, we firstly focus on the *priori* coarse-grained analysis of filtered SGS turbulent kinetic energy K^f_{sgs} to evaluate

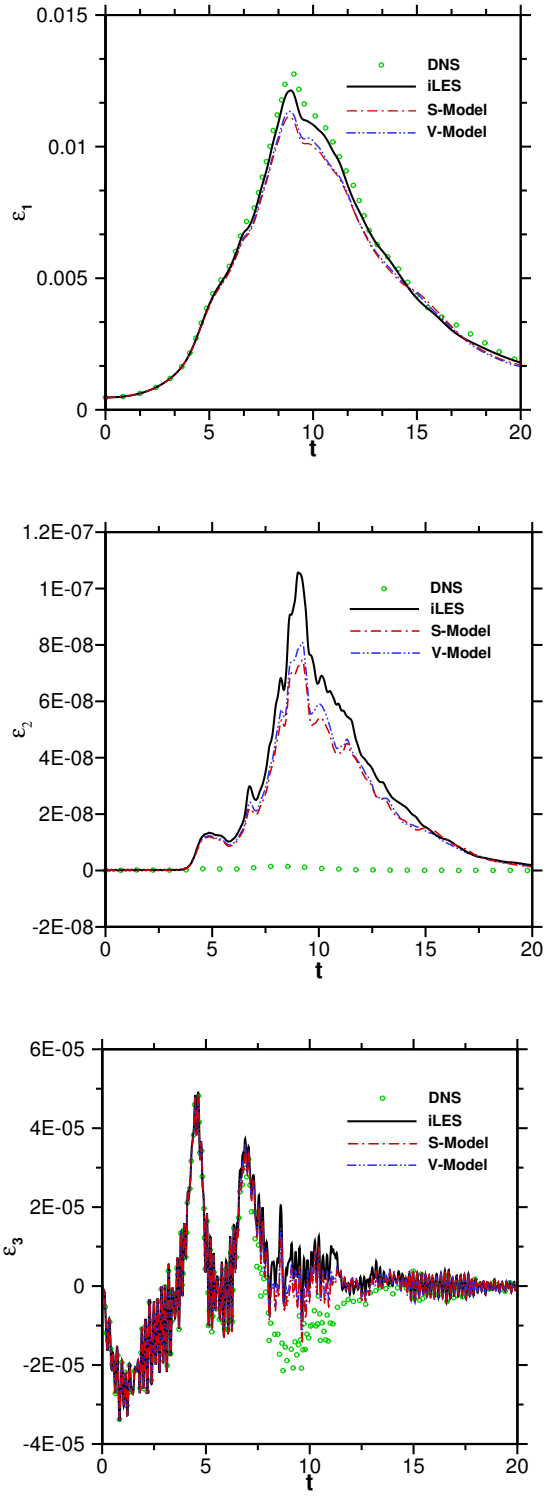

Figure 3. Time history of three contributions of ensemble physical dissipation rate ε_1, ε_2 and ε_3.

the filtered SGS production of K^f_{sgs} quantitatively. The following DNS flow-fields have been obtained as case TG_3 in Cao *et al.* (2022), where 2^3 grids are coarsen to 1 grid with Box filter. Positive definite kernel of Box filter can guarantee positive filtered SGS turbulent kinetic energy (Vreman *et al.*, 1994). After filtering process, the flow variable can be decomposed into resolved and SGS terms as $\phi(\boldsymbol{x}) = \overline{\phi}(\boldsymbol{x}) + \phi'(\boldsymbol{x})$. To avoid SGS term appearing in the filtered continuity equation,

Favre (1965) proposed the Favre (density-weighted) filtering as $\tilde{\phi} = \overline{\rho\phi}/\overline{\rho}$. Favre filtered SGS stress τ_{ij}^f and compressible filtered SGS turbulent kinetic energy $\overline{\rho}K_{sgs}^f$ are defined as $\tau_{ij}^f = \overline{\rho}(\widetilde{U_i U_j}^f - \widetilde{U}_i^f \widetilde{U}_j^f)$, $\overline{\rho}K_{sgs}^f = \tau_{kk}^f/2$.

Compressible filtered SGS turbulent kinetic energy transport equation (Cao *et al.*, 2021*a*) has been derived as

$$(\overline{\rho}K_{sgs}^f)_{,t} + (\overline{\rho}K_{sgs}^f\widetilde{U}_j^f)_{,j} = P_{sgs}^f - D_{sgs}^f + \Pi_{sgs}^f + T_{sgs}^f, \quad (12)$$

where P_{sgs}^f is the filtered SGS production term, D_{sgs}^f the filtered SGS dissipation term, Π_{sgs}^f the filtered SGS pressure dilation term, and the last term T_{sgs}^f the sum of filtered SGS diffusion terms. The detailed right-hand-side terms in Eq.(12) can be found in Cao *et al.* (2021*a*). Be of scientific interest, we pay special attention to the filtered SGS production term as

$$P_{sgs}^f = -\tau_{ij}^f \widetilde{S}_{ij}^f, \quad (13)$$

with filtered $\widetilde{S}_{ij}^f = 1/2(\widetilde{U}_{i,j}^f + \widetilde{U}_{j,i}^f)$. We know that filtered SGS production term $-\tau_{ij}^f\widetilde{S}_{ij}^f$ represents the inter-scale transfer associated with the interaction of the resolved and unresolved scales (Piomelli *et al.*, 1991).

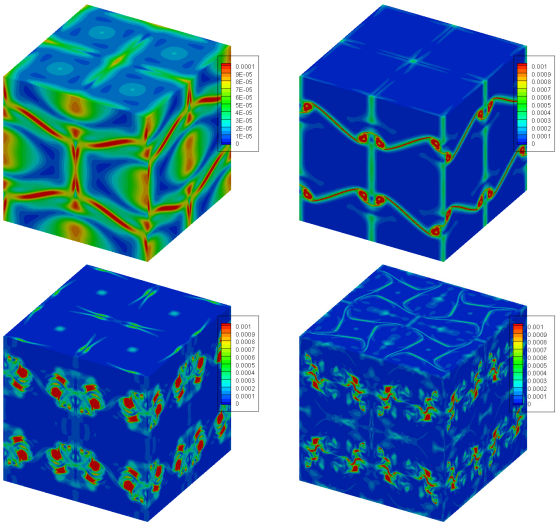

Figure 4. Filtered SGS turbulent kinetic energy K_{sgs}^f at $t = 2.5, 5, 10$ and 15.

Figure 4 qualitatively presents the contours of filtered SGS turbulent kinetic energy K_{sgs}^f. We clearly observe that K_{sgs}^f is time-dependent during the unsteady evolution process. Contours of forward and backward filtered SGS turbulent energy transfer are presented in Figure 5 and Figure 6. Forward and backward filtered SGS turbulent kinetic energy transfer is clearly observed. Filtered SGS turbulent kinetic energy backscatter illustrates the SGS turbulent kinetic energy transfer from subgrid scales to resolved scales (Piomelli *et al.*, 1991). Unfortunately, we know that backward energy transfer cannot be modeled by both iLES and eLES with static coefficients.

Table 1 quantitatively presents that E_k is in the order of $\mathcal{O}(10^4)$ to $\mathcal{O}(10^2)$ of the $\left\langle K_{sgs}^f \right\rangle$ during the evolution process. Dominant physical dissipate rate ε_1 is approximately 20 times larger than the ensemble filtered SGS production rate $\left\langle -\tau_{ij}^f \widetilde{S}_{ij}^f \right\rangle$. When constructing eLES models, the modeling SGS dissipation of eLES models is expected to be pointwise equivalent to the filtered SGS production term $-\tau_{ij}^f\widetilde{S}_{ij}^f$. As presented in Table 1, the ensemble filtered SGS production term is far smaller than the dominant ensemble physical dissipation. We know eLES always provides the positive modeling SGS dissipation without considering the numerical dissipation. However, in practical simulation, the built-in numer-

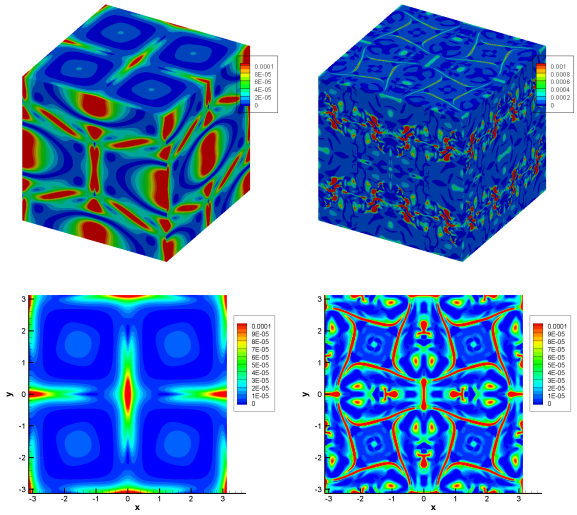

Figure 5. 3D and two-dimensional (2D) forward filtered SGS turbulent kinetic energy transfer with positive $-\tau_{ij}^f\widetilde{S}_{ij}^f$ at $t = 2.5$ and 15. Corresponding 2D slice is located at $z = 0$ plane.

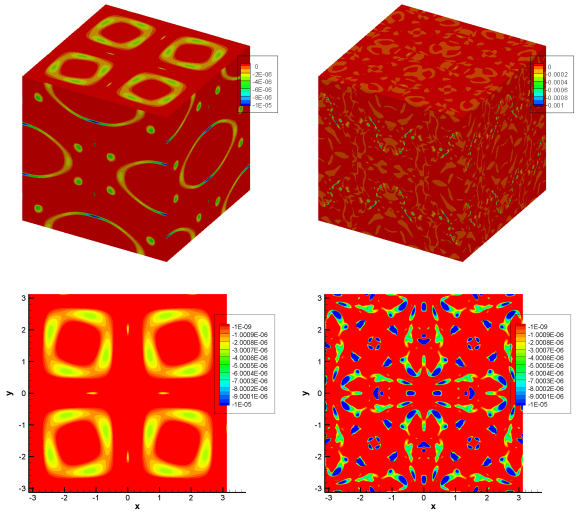

Figure 6. 3D and 2D backward filtered SGS turbulent kinetic energy transfer with negative $-\tau_{ij}^f\widetilde{S}_{ij}^f$ at $t = 2.5$ and 15. Corresponding 2D slice is located at $z = 0$ plane.

Table 1. Ensemble turbulent kinetic energy E_k, ensemble filtered SGS turbulent kinetic energy $\left\langle K_{sgs}^f \right\rangle$, ensemble dominant dissipation rate ε_1 and ensemble filtered SGS production term $\left\langle -\tau_{ij}^f \widetilde{S}_{ij}^f \right\rangle$ at $t = 2.5, 5, 10$ and 15. E_k and ε_1 are obtained from case TG_3 in Cao *et al.* (2022).

Time	E_k	$\left\langle K_{sgs}^f \right\rangle$	ε_1	$\left\langle -\tau_{ij}^f \widetilde{S}_{ij}^f \right\rangle$
2.5	0.123	2.6×10^{-5}	8.8×10^{-4}	1.3×10^{-5}
5	0.118	1.2×10^{-4}	4.1×10^{-3}	1.3×10^{-4}
10	0.074	3.3×10^{-4}	1.1×10^{-2}	5.1×10^{-4}
15	0.036	1.3×10^{-4}	4.5×10^{-3}	1.3×10^{-4}

ical dissipation always get involved with the process of total SGS dissipation. On unresolved grids, the magnitude of built-in numerical dissipation rate may be larger than the filtered SGS production rate $-\tau_{ij}^f \widetilde{S}_{ij}^f$, thus the explicit modeling SGS dissipation is not required under such circumstance. Up to this point, we have limited our discussion in *priori* analysis, and the *posteriori* performances will be evaluated thereafter.

Quantitative Analysis of SGS Dissipation

Before trusting eLES models without thinking, above *priori* analysis has reminded us to evaluate the built-in numerical dissipation quantitatively. We follow the procedures for iLES analysis in incompressible LES (Moser *et al.*, 2021). For compressible LES, without considering the numerical discrete error, the momentum equation reads

$$\frac{\partial \overline{\rho}\tilde{U}_i}{\partial t}+\frac{\partial \overline{\rho}\tilde{U}_i\tilde{U}_j}{\partial x_j}=-\frac{\partial \overline{p}}{\partial x_i}+\frac{\partial \overline{\sigma}_{ij}}{\partial x_i}-\frac{\partial \tau_{ij}}{\partial x_j}, \tag{14}$$

with SGS stress $\tau_{ij}=\overline{\rho}(\widetilde{U_iU_j}-\tilde{U}_i\tilde{U}_j)$, and $\sigma_{ij}=2\mu S_{ij}^*$ with S_{ij}^* defined as Eq.(11). Conceptually, we can define the discrete derivative operator as δ_i^t the temporal discrete derivative operator, and δ_i^s the spatial discrete derivative operator. Considering the numerical discrete error, the modified equation (numerical resolved equation) of Eq.(14) reads

$$\begin{aligned}\frac{\delta^t \overline{\rho}\tilde{U}_i}{\delta^t t}+\frac{\delta^s \overline{\rho}\tilde{U}_i\tilde{U}_j}{\delta^s x_j}=&-\frac{\delta^s \overline{p}}{\delta^s x_i}+\frac{\delta^s \overline{\sigma}_{ij}}{\delta^s x_j}-(\frac{\delta^s \tau_{ij}^{mod}}{\delta^s x_j}\\&+\frac{\delta^s \tau_{ij}^{num}}{\delta^s x_j}),\end{aligned} \tag{15}$$

where τ_{ij}^{mod} is the explicit modeling SGS stress in well-developed eLES (Nicoud & Ducros, 1999; Vreman, 2004; Sagaut, 2006; Garnier *et al.*, 2009), while all numerical discrete errors are effectively grouped into τ_{ij}^{num} phenomenologically. Numerical discrete error is very hard to analyze term by term in finite-volume framework, since the errors result from the spatial reconstruction procedure, time discretization procedure, the design of flux, and the averaging process when updating conservative variables. Another bad news is that the numerical error is grid resolution-dependent, numerical scheme-dependent and turbulence type-dependent, thus determining its quantitative expression seems mission impossible.

In view of this dilemma, we adopt to deal with the total SGS dissipation, which is a classical route to understand the eLES models in LES community. In practical simulations, corresponding to Eq.(15), the pointwise total SGS dissipation rate ε_{sgs}^p contains two parts

$$\begin{aligned}\varepsilon_{sgs}^p&=\varepsilon_{sgs}^{mod}+\varepsilon_{sgs}^{num},\\ \varepsilon_{sgs}^{mod}&=-\tau_{ij}^{mod}\tilde{S}_{ij},\\ \varepsilon_{sgs}^{num}&=-\tau_{ij}^{num}\tilde{S}_{ij}.\end{aligned} \tag{16}$$

Eq.(16) shows that the total SGS dissipative behavior is determined by both explicit modeling SGS dissipation rate ε_{sgs}^{mod} and built-in numerical SGS dissipation rate ε_{sgs}^{num}. We notice that there is no explicit modeling SGS dissipation in iLES. While, the built-in numerical dissipation is usually ignored in eLES. In terms of the free decaying TGV, ensemble total dissipation rate $\varepsilon(E_k)$ of turbulent kinetic energy and ensemble total SGS dissipation rate ε_{sgs} can be computed by

$$\begin{aligned}\varepsilon(E_k)&=-\frac{\mathrm{d}E_k}{\mathrm{d}t},\\ \varepsilon_{sgs}&\equiv\langle\varepsilon_{sgs}^p\rangle=\varepsilon(E_k)-\varepsilon_{phy},\end{aligned} \tag{17}$$

with second-order central difference method in computing $\varepsilon(E_k)$. Again, the discrete error in post-processing procedure is assumed to be neglected. ε_{phy} denotes the ensemble resolved physical dissipation rate as Eq.(11).

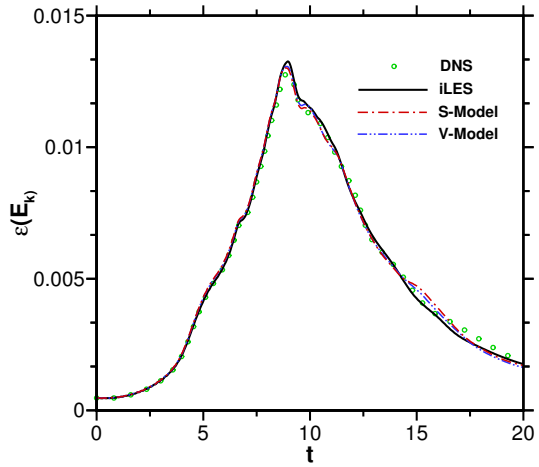

Figure 7. Time history of ensemble total dissipation rate $\varepsilon(E_k)$.

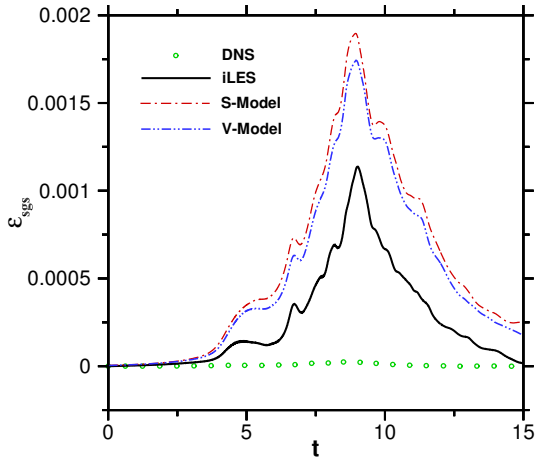

Figure 8. Time history of ensemble total SGS dissipation rate ε_{sgs}.

Table 2. Ensemble total SGS dissipation rate ε_{sgs} with iLES and eLES at $t=2.5,5,10$ and 15.

Time	iLES	S-Model	V-Model
2.5	1.5×10^{-5}	2.8×10^{-5}	2.6×10^{-5}
5	1.4×10^{-4}	3.5×10^{-4}	3.2×10^{-4}
10	6.7×10^{-4}	1.4×10^{-3}	1.3×10^{-3}
15	1.8×10^{-5}	2.5×10^{-4}	1.8×10^{-4}

Figure 7 shows that $\varepsilon(E_k)$ is well predicted at all grid levels by iLES and eLES, indicating that the resolved physical dissipation and total SGS dissipation work together consistently in the calculation. Thence, the numerical dissipation in iLES indeed can be treated as the built-in SGS dissipation. As presented in Figure 1 - 3, the built-in numerical SGS dissipation accounts for the reasonable performance of iLES in current low-Reynolds number compressible turbulence. Figure 8 shows that the ensemble total SGS dissipation rate ε_{sgs}

based on eLES is approximate 2 times larger than that of iLES, because the static eddy viscosity model always provides the positive modeling SGS dissipation. Additionally, we observe that the *posteriori* ensemble total SGS dissipation rate ε_{sgs} in Table 2 is larger than the *priori* ensemble filtered SGS production term $\left\langle -\tau_{ij}^{f}\widetilde{S}_{ij}^{f}\right\rangle$ in Table 1, except for the late decaying stage at $t = 15$. We revisit the time history of ensemble enstrophy dissipation rate $\varepsilon(\zeta)$ in Figure 2. We can conclude that the additional explicit models in eLES pollutes the resolved turbulent structures, i.e., blurs the resolution of resolved vorticity. To strengthen above conclusion, effects of static eddy viscosity models on density, momentum and energy transport will be explored, beyond grouping the explicit modeling effects into the effective ensemble modeling SGS dissipation.

CONCLUSION AND DISCUSSION

To address the better performance of iLES, current research conducts the quantitative comparisons between iLES and eLES, especially focusing on the built-in numerical dissipation and explicit modeling SGS dissipation. It is concluded that the numerical dissipation in iLES can act as the intrinsic SGS dissipation, and explicit modeling SGS dissipation is not required in low-Reynolds number turbulence. In addition, the additional explicit SGS models in eLES even pollute the resolved turbulent structures. An important consequence is that the improvement of the reliability of LES results requires work on both the numerical methods and the subgrid models.

In following studies, more detailed analysis in Eq.(15) deserves to be explored. iLES for complex turbulent flows is still under debate, current quantitative analysis of total SGS dissipation gives the specific hints on this issue. More importantly, the LES community should pay special attention to the utilization of static explicit eddy viscosity models, instead of regarding the eLES as holy grail in LES on unresolved grids.

REFERENCES

Bhatnagar, Prabhu Lal, Gross, Eugene P & Krook, Max 1954 A model for collision processes in gases. i. small amplitude processes in charged and neutral one-component systems. *Physical review* **94** (3), 511.

Boris, Jay P, Grinstein, Fernando F, Oran, Elaine S & Kolbe, Ronald L 1992 New insights into large eddy simulation. *Fluid dynamics research* **10** (4-6), 199.

Brachet, Marc E, Meiron, Daniel I, Orszag, Steven A, Nickel, BG, Morf, Rudolf H & Frisch, Uriel 1983 Small-scale structure of the taylor–green vortex. *Journal of Fluid Mechanics* **130**, 411–452.

Cao, Guiyu, Pan, Liang & Xu, Kun 2021*a* Three dimensional high-order gas-kinetic scheme for supersonic isotropic turbulence ii: Coarse-graining analysis of compressible ksgs budget. *Journal of Computational Physics* **439**, 110402.

Cao, Guiyu, Pan, Liang & Xu, Kun 2022 High-order gas-kinetic scheme with parallel computation for direct numerical simulation of turbulent flows. *Journal of Computational Physics* **448**, 110739.

Cao, Guiyu, Xu, Kun, Pan, Liang & Chen, Shiyi 2021*b* High-order gas-kinetic scheme in general curvilinear coordinate for iles of compressible wall-bounded turbulent flows. *arXiv preprint arXiv:2107.08609* .

Chapman, Sydney & Cowling, Thomas George 1990 *The mathematical theory of non-uniform gases: an account of the kinetic theory of viscosity, thermal conduction and diffusion in gases*. Cambridge university press.

DeBonis, James 2013 Solutions of the taylor-green vortex problem using high-resolution explicit finite difference methods. In *51st AIAA Aerospace Sciences Meeting including the New Horizons Forum and Aerospace Exposition*, p. 382.

Favre, Alexandre 1965 Equations des gaz turbulents compressibles. *J. de Mecanique* **4** (3).

Gallis, MA, Bitter, NP, Koehler, TP, Torczynski, JR, Plimpton, SJ & Papadakis, G 2017 Molecular-level simulations of turbulence and its decay. *Physical review letters* **118** (6), 064501.

Garnier, Eric, Adams, Nikolaus & Sagaut, Pierre 2009 *Large eddy simulation for compressible flows*. Springer Science & Business Media.

Grinstein, Fernando F, Margolin, Len G & Rider, William J 2007 *Implicit large eddy simulation*, , vol. 10. Cambridge university press Cambridge.

Kumar, G, Girimaji, Sharath S & Kerimo, J 2013 Weno-enhanced gas-kinetic scheme for direct simulations of compressible transition and turbulence. *Journal of Computational Physics* **234**, 499–523.

Li, Jiequan & Du, Zhifang 2016 A two-stage fourth order time-accurate discretization for lax–wendroff type flow solvers i. hyperbolic conservation laws. *SIAM Journal on Scientific Computing* **38** (5), A3046–A3069.

Lombard, Jean-Eloi W, Moxey, David, Sherwin, Spencer J, Hoessler, Julien FA, Dhandapani, Sridar & Taylor, Mark J 2016 Implicit large-eddy simulation of a wingtip vortex. *AIAA Journal* **54** (2), 506–518.

Manabe, Syukuro, Smagorinsky, Joseph & Strickler, Robert F 1965 Simulated climatology of a general circulation model with a hydrologic cycle. *Monthly Weather Review* **93** (12), 769–798.

Moser, Robert D, Haering, Sigfried W & Yalla, Gopal R 2021 Statistical properties of subgrid-scale turbulence models. *Annual Review of Fluid Mechanics* **53**, 255–286.

Nicoud, Franck & Ducros, Frédéric 1999 Subgrid-scale stress modelling based on the square of the velocity gradient tensor. *Flow, turbulence and Combustion* **62** (3), 183–200.

Pan, Liang, Xu, Kun, Li, Qibing & Li, Jiequan 2016 An efficient and accurate two-stage fourth-order gas-kinetic scheme for the euler and navier–stokes equations. *Journal of Computational Physics* **326**, 197–221.

Piomelli, Ugo, Cabot, William H, Moin, Parviz & Lee, Sangsan 1991 Subgrid-scale backscatter in turbulent and transitional flows. *Physics of Fluids A: Fluid Dynamics* **3** (7), 1766–1771.

Sagaut, Pierre 2006 *Large eddy simulation for incompressible flows: an introduction*. Springer Science & Business Media.

Vreman, AW 2004 An eddy-viscosity subgrid-scale model for turbulent shear flow: Algebraic theory and applications. *Physics of fluids* **16** (10), 3670–3681.

Vreman, Bert, Geurts, Bernard & Kuerten, Hans 1994 Realizability conditions for the turbulent stress tensor in large-eddy simulation. *Journal of Fluid Mechanics* **278**, 351–362.

Xu, Kun 2001 A gas-kinetic bgk scheme for the navier–stokes equations and its connection with artificial dissipation and godunov method. *Journal of Computational Physics* **171** (1), 289–335.

Xu, Kun 2015 *Direct modeling for computational fluid dynamics: construction and application of unified gas-kinetic schemes*. World Scientific.

Zhao, Wenjin, Wang, Jianchun, Cao, Guiyu & Xu, Kun 2021 High-order gas-kinetic scheme for large eddy simulation of turbulent channel flows. *Physics of Fluids* **33** (12), 125102.